RadPhi TechNote
RadPhi-2000-801

Timing Calibration

Russell Mammei and Elton Smith
August 17, 2000

We describe the timing calibration procedures for the tagger spectrometer for experiment E94-016 (RadPhi). The goal of experiment E94-016, which collected data this past summer in Hall B of the Thomas Jefferson National Accelerator Facility (JLab), is to measure the branching ratios for rare radiative decays of the phi meson, including $\phi \to f_0(975)\gamma \to \pi^0\pi^0\gamma$, $\phi \to a_0(980)\gamma \to \pi_0\eta\gamma$, and $\phi \to \eta'\gamma$. Each tagger T-counter and BSD T-counter was referenced to one charged particle veto (CPV) counter. This is possible because the mixture of the reactions in the CPV are similar for different tagger counters. These calibrations will allow the RadPhi collaboration to tighten the cuts in the data analysis and thereby enhance signal events relative to background.

1 Setup

RadPhi employs five main detectors, Lead Glass calorimeter (LGD), Barrel Scintillator Detector (BSD), Barrel Gamma Veto, and the Charged Particle Veto (CPV), in concert with the photon tagger in Hall B of JLab. A continuous wave electron beam of approximately 5.65 GeV is delivered into the hall and hits a gold foil radiator situated inside the tagger. A bremsstrahlung photon beam is produced and travels down the beam path along with the residual electron beam. The electrons of the beam are then deflected via a magnetic field to hit one of the 18 tagger scintillator detectors, while the photon beam proceeds unscathed. The photon beam travels down stream through the CEBAF Large Acceptance Spectrometer (CLAS) and into the RadPhi detection system, where the photon beam interacts with the protons of a solid beryllium target. The setup is shown schematically in Fig. 1.

A three-level trigger was developed to isolate these reactions. The first level trigger is a combination of four criteria that must be met before a computer system temporarily freezes, and later records interesting information from each detector subsystem. This is called an event. The detectors are continuously looking for these criteria: tagger signal, UPV signal in anti-coincidence, BSD signal, and a LGD signal. Once these criteria are met the signals must pass a second and third level trigger which is dependent on the energy deposited in the LGD. If the event passes all three triggers the event is recorded.

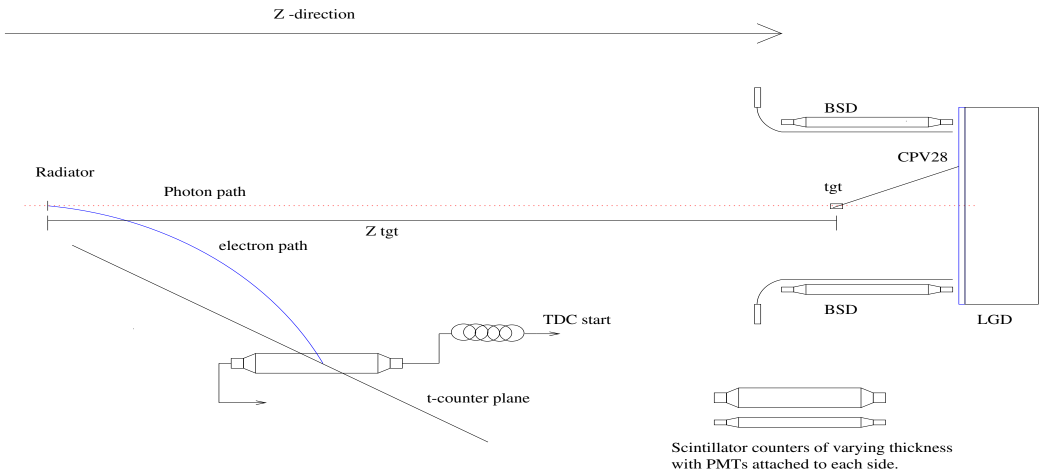

Figure 1: Schematic of detector hits in tagger and detector.

2 Charged Particle Veto

The Charged Particle Veto detects charged particles, e.g. π^+, and is located immediately upstream of the Lead Glass Detector. The CPV consists of 30 scintillator panels aligned horizontally. See Fig. 2. CPV 28 was chosen as the reference because of its high coincidence rate with tagger hits. See Fig. 3. The time recorded by the CPV in ns is given in Eq. 1:

$$t_{cpv} = \frac{(z_{tgt} - z_{rad})}{c} + \frac{\sqrt{(z_{cpv} - z_{tgt})^2 + x_{cpv}^2 + y_{cpv}^2}}{\beta c} + \frac{l_{cpv} - |x_{cpv}|}{v_{eff}^{cpv}} + c_1 D_{cpv} \quad (1)$$

The time for the photon to get to the target is represented by $(z_{tgt} - z_{rad})/c$, while the time for the charged particle to get to the CPV is given by $\sqrt{(z_{cpv} - z_{tgt})^2 + x_{cpv}^2 + y_{cpv}^2}/\beta c$. Note that y_{cpv}^2 is constant. The third term gives the signal propagation time through the scintillator of length l_{cpv}, and the all electronic delays are lumped into $c_1 D_{CPV}$. Here βc is the velocity of the particle hitting the CPV, ($0 \leq \beta \leq 1$) and v_{eff}^{CPV} is the velocity of light propagation in the scintillator, approximately 16cm/ ns. Therefore the time of the CPV in terms of TDC counts is given by Eq. 2:

$$T_{cpv} = T_{stop} + \frac{t_{cpv}}{c_1} \quad (2)$$

Which becomes Eq. 3:

$$T_{cpv} = T_{stop} - \frac{z_{tgt} - z_{rad}}{c c_1} - \frac{\sqrt{(z_{cpv} - z_{tgt})^2 + x_{cpv}^2 + y_{cpv}^2}}{\beta c c_1} - \frac{l_{cpv} - |x_{cpv}|}{v_{eff}^{cpv} c_1} - D_{cpv} \quad (3)$$

3 Photon Tagger

The role of the tagger is to create a bremsstrahlung photon beam, to determine the energy of that photon beam, and is useful to over-constrain the kinematics of

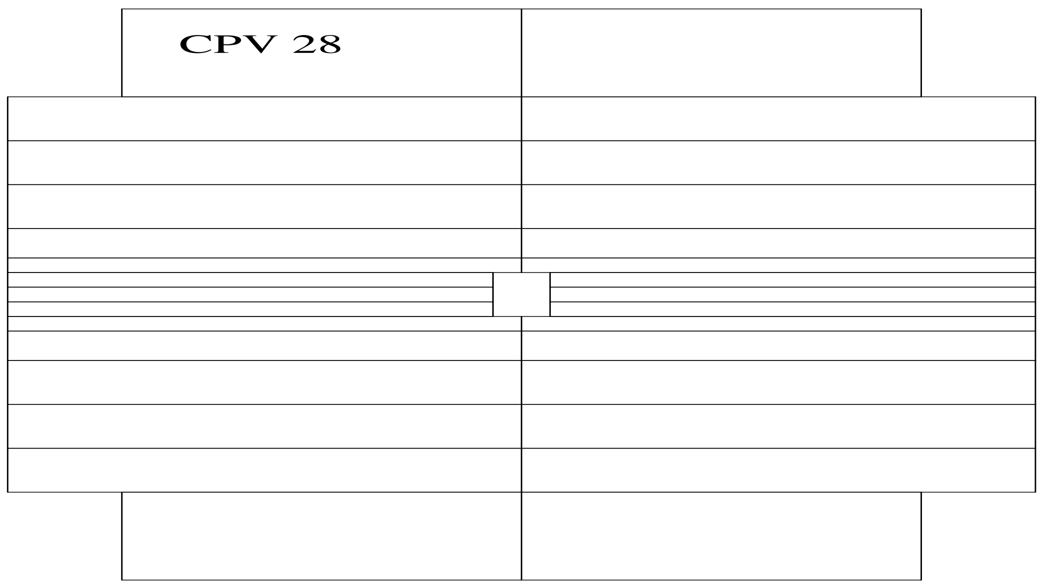

Figure 2: Frontal view of the CPV showing the 30 counters, including the reference CVP28.

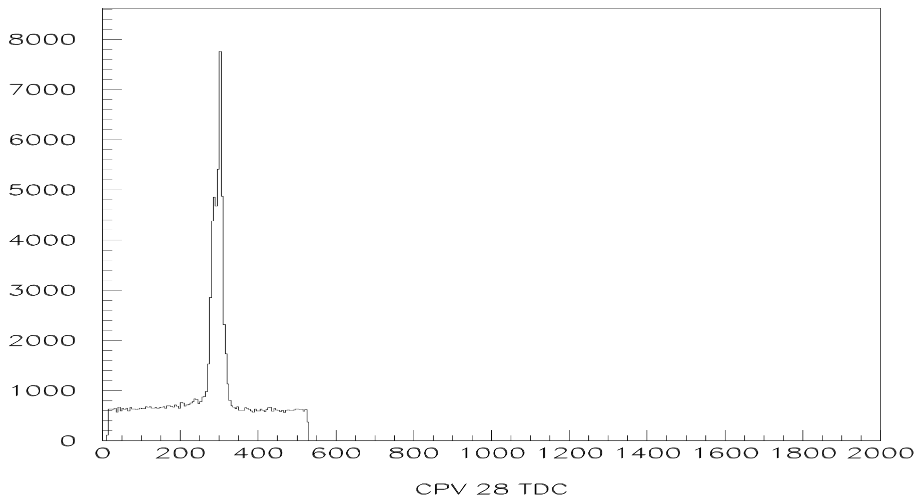

Figure 3: Time of CPV 28 relative to the Trigger. The peak corresponds to hits in the CPV which are in-time with interactions in the RadPhi target.

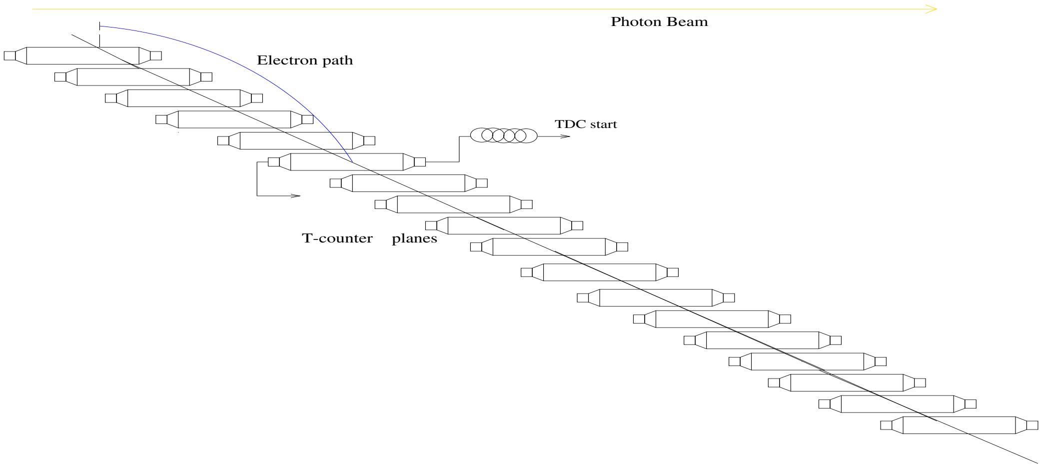

Figure 4: Schematic of the photon tagger scintillator counters.

the event. Precise determination of the photon energy is imperative and the timing calibrations allow to determine corresponding tagger and detector information. The energy of the electron is determined by the position of the counter with the electron hit. See Fig. 4. The T-counters are numbered such that a high T-counter number corresponds to a low photon energy. If the electron hits the higher number counters, then the corresponding photon has low energy in relation to the initial energy of the electron. If the electron hits a low T-counter number, then its corresponding photon has higher energy.

When the electron hits the T-counter scintillators, scintillator light is produced isotropically, which is collected by two PMTs attached to the ends of each scintillator detector. The PMTs turn the photons into electrons and boost the signal on the order of 10^6, which then activates the TDC start time. In essence, each hit in the T-counters creates a timing signature which is then passed through the first level trigger.

We take the time the electron beam hits the radiator as t_{rad}=0, and write all times relative to this time. See Fig.2.

4 Tagger Timing

A hit in the left PMT of a tagger T-counter is given by

$$t_{tag} = c_1 D^L_{tag} + \frac{l_{path}}{c} \tag{4}$$

A similar expression is valid for the right side, and the superscript L is replaced by R. Electronic delays are lumped into the constant D_{tag}, which is different from counter to counter. The purpose of the calibration procedure is to determine these delays relative to one another. This delay is given in terms of TDC counts, which can be converted to ns using the expression in Eq. 5:

$$\begin{aligned} time(ns) &= \text{offset} + c_1 \times TDC(counts) \quad (5) \\ c_1 &= 0.5\ ns/count \quad (6) \end{aligned}$$

Relative time for each T-counter is obtained by taking the time in the tagger and subtracting the time of the CPV. Producing Eq.7:

$$\begin{aligned} T^L_{tag} - T_{cpv} &= (-D^L_{tag} + D_{cpv}) + [\frac{z_{tgt} - z_{rad}}{c_1 c}] + \frac{\sqrt{(z_{cpv} - z_{tgt})^2 + x^2_{cpv} + y^2_{cpv}}}{\beta c c_1} \\ &+ \frac{l_{cpv} - |x_{cpv}|}{v^{cpv}_{eff} c_1} \quad (7) \end{aligned}$$

The second term on the right side of the equation is a calculable constant and the last two terms become approximately constant when averaged over many events. Thus by plotting the difference between the TDC times and the time from CPV, the electronic delays may be determined.

5 Histograms

By modifying parse.c of the analysis package RODD, histograms of the tagger T-counter time relative to the in-time hits in CPV 28 were created. Events with times in CPV 28 within ± 50 counts of the coincidence peak were considered.

The resulting peaks were then processed through a kumac file [1] that fitted them, plotted them, and created a data file containing each tagger number and the corresponding means and sigmas of the fits. A constant, with starting value of 10, was used to fit the background and the function sigma (LVMAX) provided the starting mean for the Gaussian fit of the peak. (This function scans the histogram vector for the channel with the largest bin number and records this number.) The following histograms were produced. See Fig. 5 and 6.

6 Uploading into maps

To make these timing changes available a parsing code was written that would upload the values of each peak into the Hitmaps analysis package. Dat_put.c was checked out from the RadPhi software repository and modified to upload the constants according to run number. A graduate student from Indiana University, Craig Steffen, developed the following procedure to upload the constants into the map (emphasized text indicates keyboard input):

1. *cvsCheckout taggerdata*

2. *cvsCheckout config*

[1]/home/mammei/radphi/paw/rodd_tagger_ref.kumac

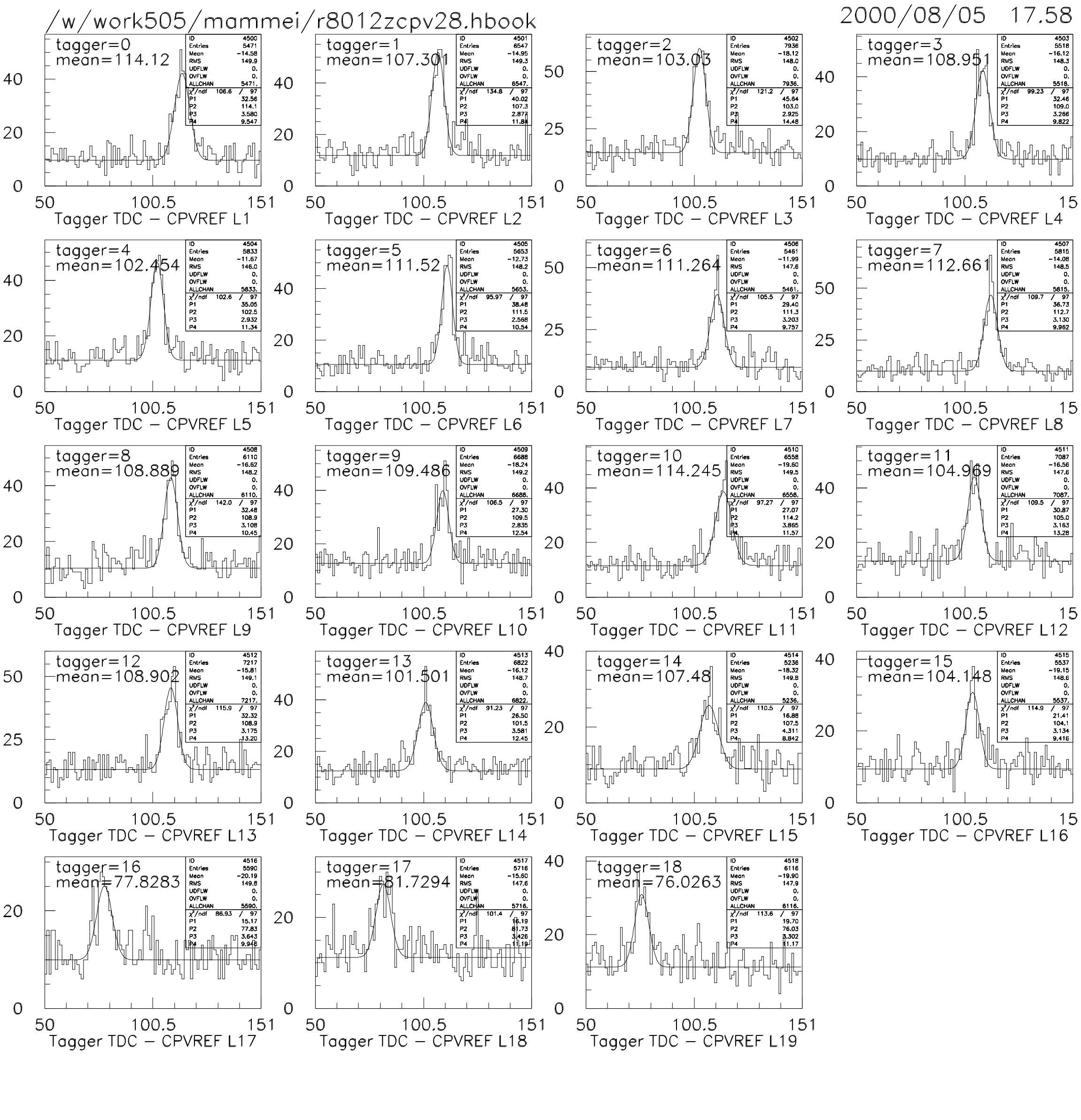

Figure 5: Plots and Fits of the Left Tagger TDC counters.

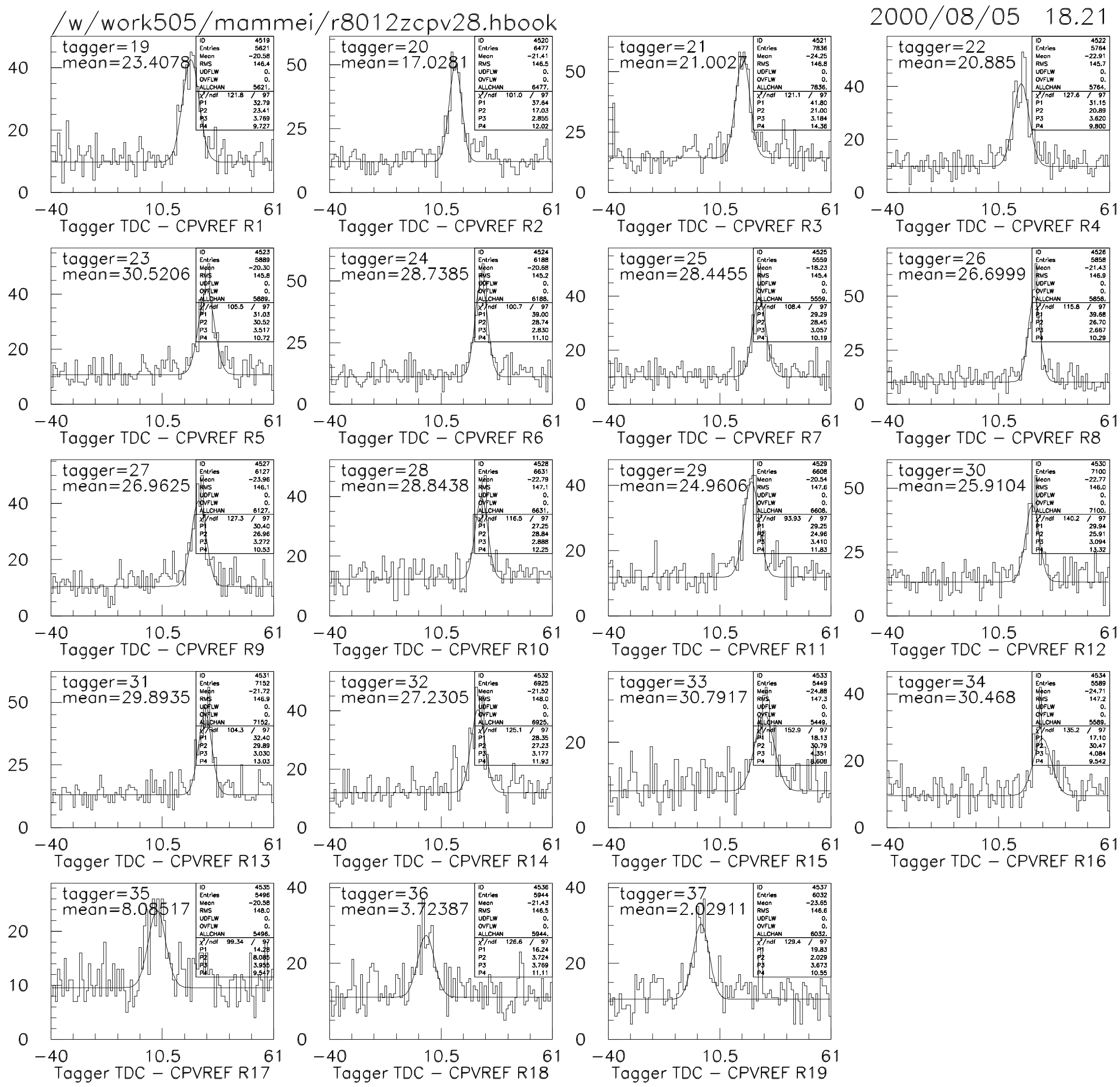

Figure 6: Plots and Fits of the Right Tagger TDC counters.

3. modify data_put.c according to how you set up your files.

4. *make data_put*

5. *setenv RADPHI_CONFIG [your_user_name/config]*

6. *data_put [the run_number] [the name of your data file]* e.g. *data_put 8888 taggermean8888.dat* (This uploads the new constants into your local version of the map. Your numbers can be checked by using mapdump on the map you have modified.)

7. *cd*

8. *cd config/maps*

9. *cvsCommit [detector_params.map]* (or whichever map is appropriate)

10. enter a comment on the map you just altered.

11. press <control>d

This process uploads the delay constants into the maps in the Radphi home directory where they can be used to produce more intricate cuts on the raw data.

7 Interpretation of plots

Ten standard trigger runs beginning with r7871 and ending with r8444 were analyzed and uploaded into the maps. The cabling of the T-counters in groups of 16 is observed in the measured delays. T-counters 1-16 correspond to one connector, and 17 through 19 correspond to a second one. See Fig 5 and 6. The average width (sigma) for each fit is approximately 3 channels (1.5 ns). This is due to the intrinsic resolution in the CPV, not the tagger. The intrinsic resolution of the tagger was determined by taking the difference between the corresponding left and right T-counters and fitting these peaks. See Fig. 7. The fitted plots show an average sigma of 1 channel (0.5 ns), which is the specified resolution of the 1877 TDCs. Therefore the width of the peaks in the tagger-cpv28 fits are dominated by the intrinsic resolution in the CPV.

In order to determine a timing change between the runs, a kumac file [2] was produced that subtracted the two histograms and plotted their difference. Two major timing changes were discovered between runs r7871 to r8444. The first timing change of 94 channels occurred between runs r8147 and r8154. See Fig. 8. The second timing change of 5 channels occurred between runs r8177 and r8222. See Fig. 9. These changes agree with modifications to the electronic setup (RadPhi logbook volume VIII). Thus the runs can be grouped by hardware change into Table 1.

[2] /home/mammei/radphi/paw/russmean.kumac

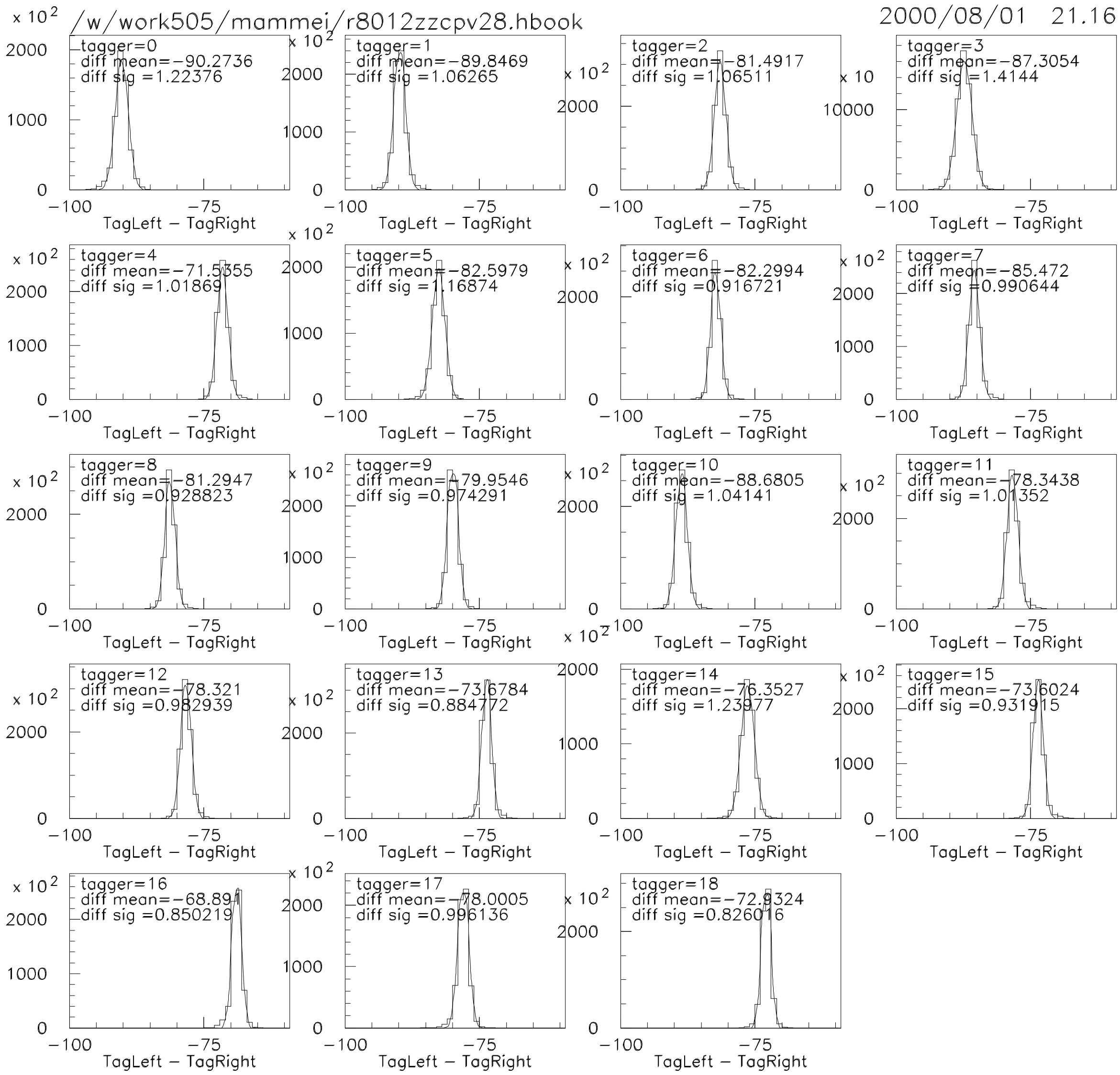

Figure 7: T-counter(Left) - T-counter(Right) plot showing tagger intrinsic resolution.

Table 1: **Constant change blocks.**

Period 1	Period 2	Period 3
r7871	r8154	r8222
r8012	r8163	r8347
r8138	r8177	r8444
r8147		

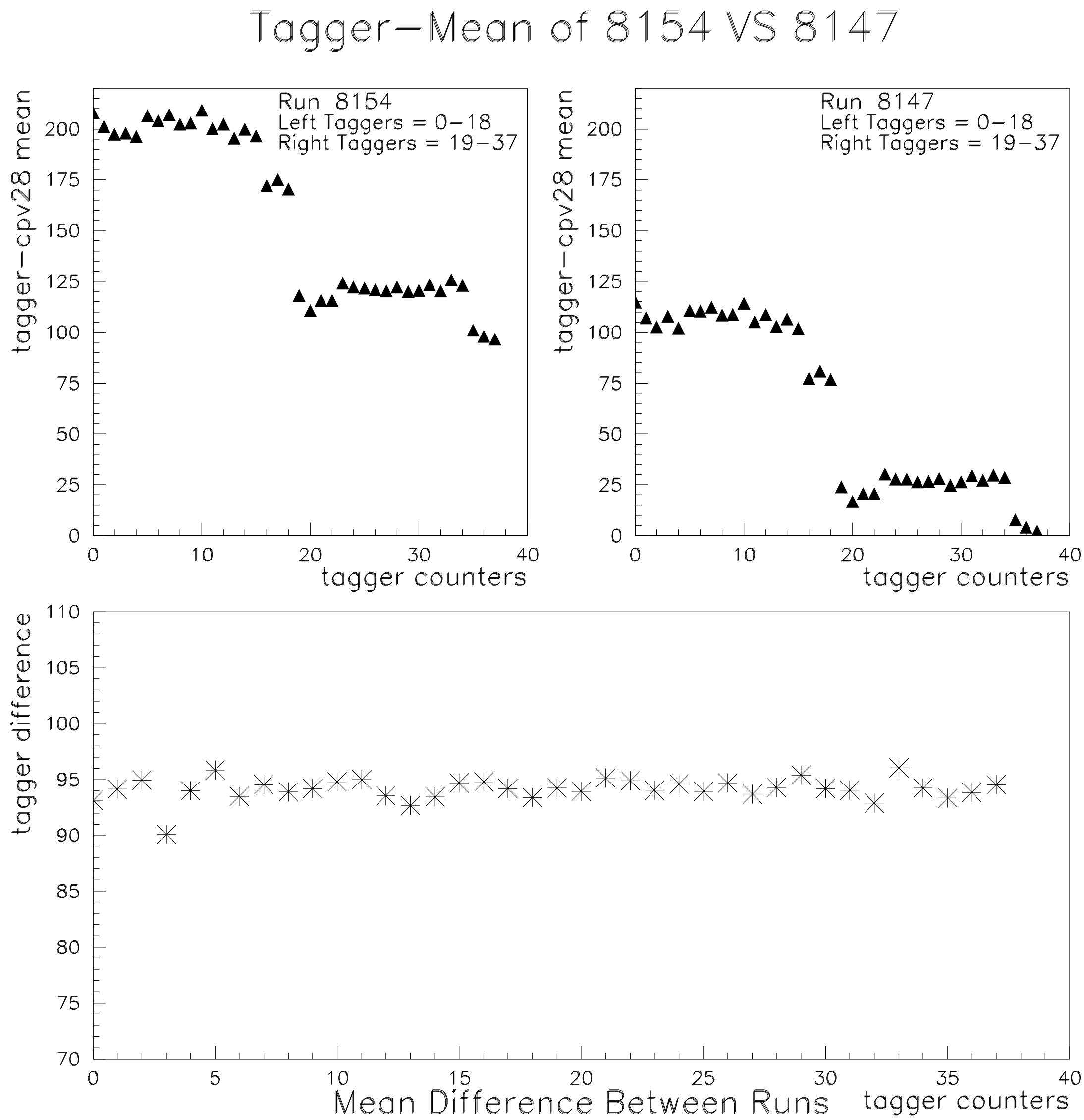

Figure 8: Comparison of runs r8154 and r8147 showing a hardware change.

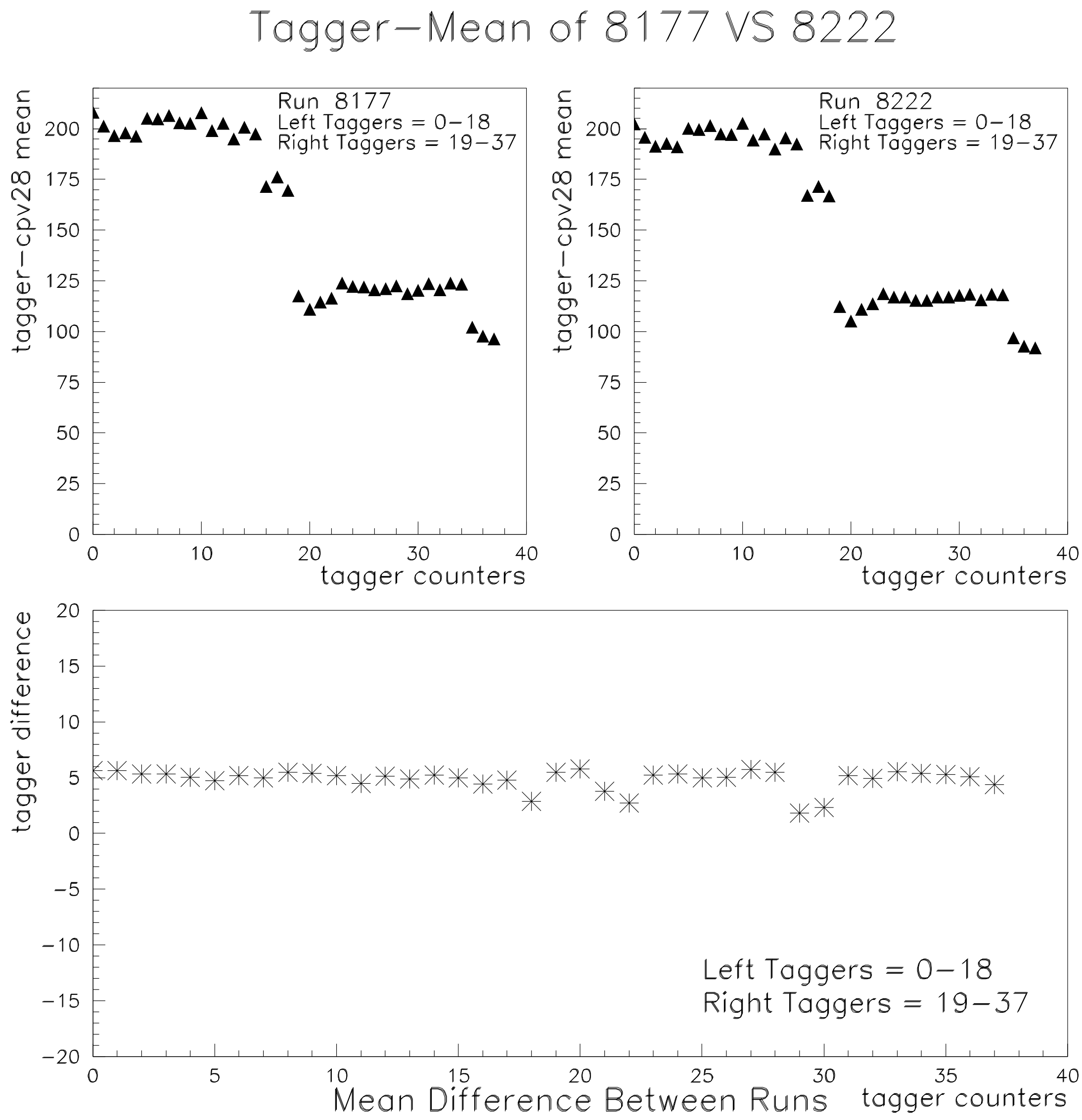

Figure 9: Comparison of runs r8177 and r8222 showing a hardware change.

8 Low-Intensity Runs

In addition to standard data runs (70 nA), we took calibration runs at low current (∼2 nA). These runs should produce a well defined peak to background ratio. Runs r8296, r8352, r8573, and r8574 have been analyzed. The histograms of r8573 are shown in Fig. 10 and 11. These runs typically contain low statistics and therefore a kumac file[3] was developed to add the runs together. However, even combining runs together we were not able to achieve the statistics of normal data runs.

9 Remaining Work

While comparing histograms together certain tagger T-counters were 4 or 5 channels apart for almost every comparison. These channels might be miss-cabled. However unlikely this might be, these discrepancies require an investigation. Until this investigation, the low-intensity analyses will not provide much information on the timing delays. Also, the official data set of usable data begins with r7415 and ends with run r8721. Due to unforeseen complications within the data and with computer programs only 44% of the usable data have delay constants. Histograms for runs r7415, r7416, r7625, and r7626 have been produced to determine these constants, but due to the lack of statistics and time constraints these delay constants have not yet been determined.

10 Conclusion

Time delay constants for the photon tagger T-counters have been determined for 44% of the usable data for the RadPhi experiment (runs r7871 to r8444). CPV 28 was chosen as the reference because of its high coincidence rate with the tagger. The hits in this peak were subtracted from the in-time hits of each tagger T-counter. These histograms were produced by the analysis package RODD and the resulting peaks were plotted and fitted with the use of PAW. The means of these fits were then uploaded into the RadPhi detector maps, via a parsing code.

Two hardware changes were discovered; one between runs r8147 and r8154, the other between r8177 and r8222 with a change of 94 bins (47 ns) and 5 bins(2.5 ns) respectively. An analysis of low-intensity runs along with the determination of the rest of the delay constants for the usable data set will complete this project.

A Timing for Other Detectors

While we have only calibrated the timing of the tagger counters, we have considered the issues associated with obtaining calibrations for other subsystems as well. In this appendix we present some ideas for the strategy of calibrating other subsystems which are important to obtaining a picture of the timing for the entire detector.

[3] /home/mammei/paw/rodd_tagger_pass1.kumac

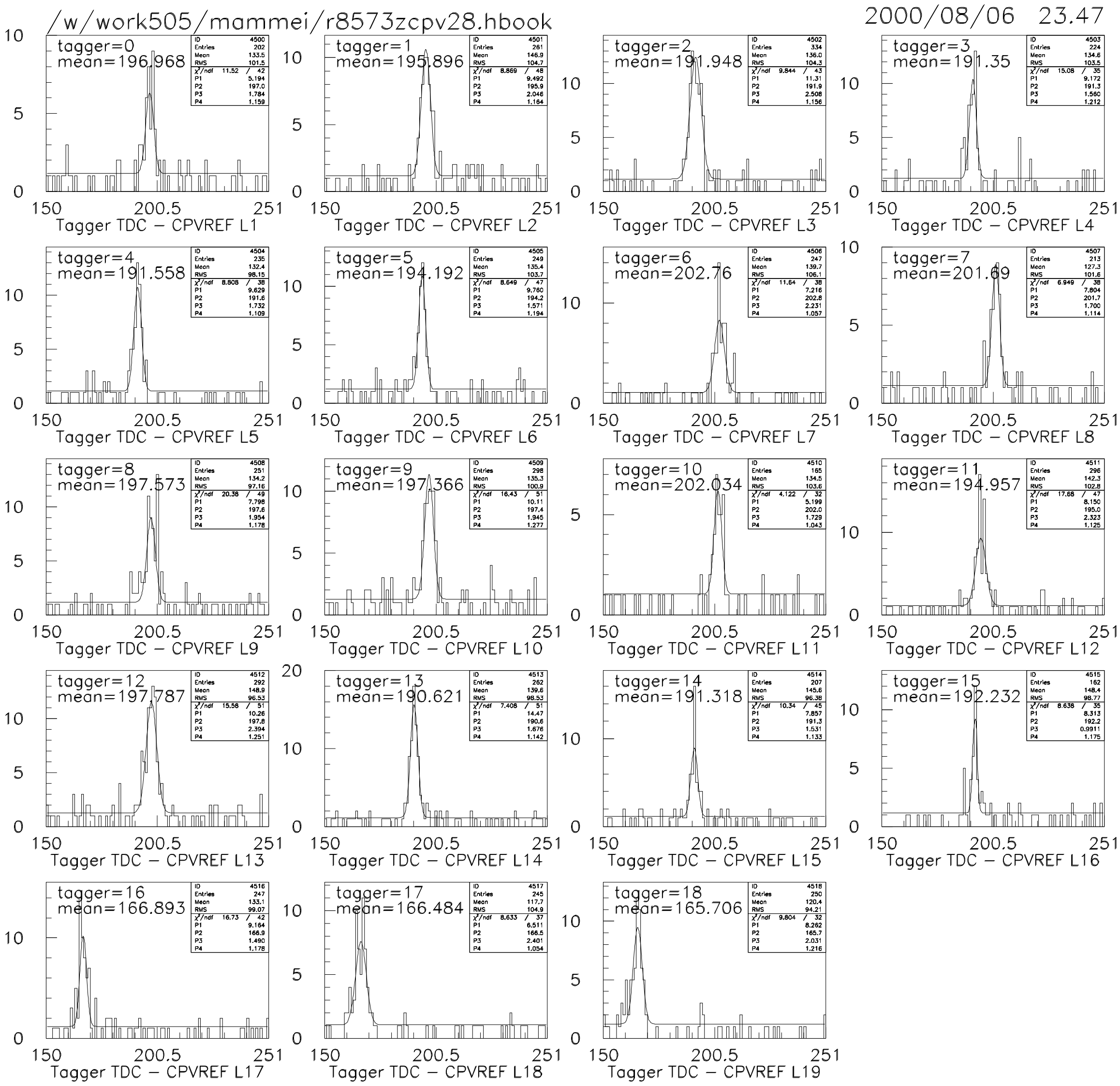

Figure 10: Plots and Fits of the Left T-counters for Low-Intensity Run r8573.

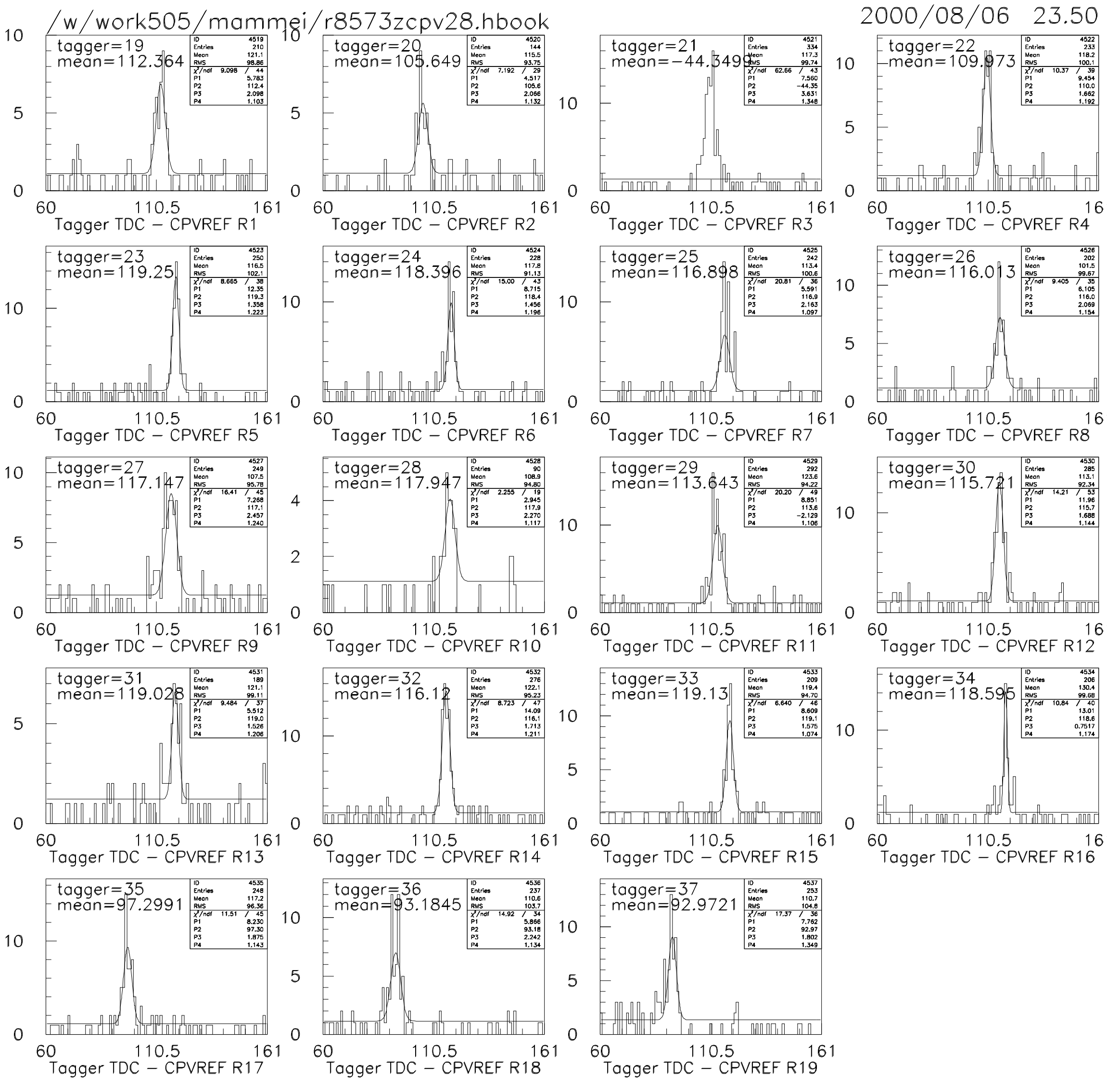

Figure 11: Plots and Fits of the Rights T-counters for Low-Intensity Run r8573.

A.1 Barrel Scintillator Detector

The time of the hits in the Barrel Scintillator Detector (BSD) are given in Eq. 8 by the transit time of the photon from the radiator to the target, flight time of the particle from the target to the BSD, the time for scintillation light to travel from the point of impact to the PMT, explicit slewing due to time-walk, and delays in the cables and electronics:

$$\begin{aligned} t_{BSD} &= \frac{(z_{tgt} - z_{rad})}{c} + \frac{\sqrt{R_{BSD}^2 + (z_{hit} - z_{tgt})^2}}{\beta c} + \frac{z_{hit}}{v_{eff}^{BSD}} \\ &+ \frac{C_{walk}^{BSD}}{\sqrt{a_{BSD}}} + c_1 D_{BSD} \end{aligned} \tag{8}$$

Here a_{BSD} is the pedestal-subtracted value of the ADC in the BSD. The velocity β of the particle traveling from the target to the BSD is generally unknown. For the experimental signal, this particle would be a proton and its velocity would vary for different kinematics, depending primarily on the proton recoil angle, but also depending on the incident photon energy and whether one produces a ϕ or an ω. For ϕ production, β varies from 0.15 to 0.7 for recoil angles between 40 and 60 degrees. For ω production the velocities can be as low as 0.1. For $R_{BSD} = 36$ cm, this corresponds to flight times of between 1.7 to 12 ns. To determine the time of impact one should fix z_{hit} (by specifying a pixel hit), and can use this also to estimate the velocity of the scattered proton, assuming a particular reaction. We note that typical triggers may include a range of particles and kinematics, so they might not reproduce the timing of interesting signal events. Therefore accurate timing might require a selection of kinematically over-determined events.

A.2 Barrel Gamma Veto

The timing of the upstream PMTs of the BGV is given by Eq. 9:

$$\begin{aligned} t_{BGV}^{U} &= \frac{(z_{tgt} - z_{rad})}{c} + \frac{\sqrt{R_{BGV}^2 + (z_{hit} - z_{tgt})^2}}{\beta c} \\ &+ \frac{z_{hit}}{v_{eff}^{BGV}} + \frac{C_{walk}^{BGV,U}}{\sqrt{a_{BGV}}} + c_1 D_{BGV}^{U} \end{aligned} \tag{9}$$

Where the time-walk correction function f_W (see Section A.3 below) is a function of the pulse height a_{BGV}, but also depends on calibration constants C_{BGV}, which may be difficult to extract directly from the data. We may need to use estimates, at least for the initial round of calibrations.

The down stream timing for the BGV is given by Eq. 10

$$\begin{aligned} t_{BGV}^{D} &= \frac{(z_{tgt} - z_{rad})}{c} + \frac{\sqrt{R_{BGV}^2 + (z_{hit} - z_{tgt})^2}}{\beta c} \\ &+ \frac{(l_{BGV} - z_{hit})}{v_{eff}^{BGV}} + \frac{C_{walk}^{BGV,D}}{\sqrt{a_{BGV}}} + c_1 D_{BGV}^{D} \end{aligned} \tag{10}$$

The same note on the time-walk correction function f_W for the upstream PMTs applies here. Note however, that the time-walk calibration constants are not necessarily equal, and in fact due to the construction of the BGV we may expect upstream and downstream corrections to differ.

If we average the upstream and downstream times we obtain Eq. 11. We note that this average has the feature that it eliminates the primary dependence on z_{hit}, and makes it a useful quantity for calibration.

$$\begin{aligned}
\frac{1}{2}(t^U_{BGV} + t^D_{BGV}) &= \frac{(z_{tgt} - z_{rad})}{c} + \frac{\sqrt{R^2_{BGV} + (z_{hit} - z_{tgt})^2}}{\beta c} \\
&\quad + \frac{l_{BGV}}{2\ v^{BGV}_{eff}} + \frac{1}{2}\left(\frac{C^{BGV,U}_{walk}}{\sqrt{a_{BGV}}} + \frac{C^{BGV,D}_{walk}}{\sqrt{a_{BGV}}}\right) + \\
&\quad \frac{1}{2}(c_1 D^U_{BGV} + c_1 D^D_{BGV}) \qquad (11)
\end{aligned}$$

The mean difference is given by equation 12:

$$\begin{aligned}
\frac{1}{2}(t^U_{BGV} - t^D_{BGV}) &= \frac{z_{hit}}{v^{BSD}_{eff}} - \frac{l_{BGV}}{2\ v^{BGV}_{eff}} + \frac{1}{2}\left(\frac{C^{BGV,U}_{walk}}{\sqrt{a_{BGV}}} - \frac{C^{BGV,D}_{walk}}{\sqrt{a_{BGV}}}\right) \\
&\quad + \frac{1}{2} c_1 (D^U_{BGV} - D^D_{BGV}) \qquad (12)
\end{aligned}$$

Let us redefine our variables using sums and differences:

$$\overline{D_{BGV}} = \frac{1}{2}(D^U_{BGV} + D^D_{BGV}) \qquad (13)$$

$$\Delta D_{BGV} = \frac{1}{2}(D^U_{BGV} - D^D_{BGV}) \qquad (14)$$

The timing of this detector relative to the other subsystems is primarily determined by $\overline{D_{BGV}}$, which can be determined from the calibration of the average time only. Thus the main goal of the calibration for this system is to determine these constants, one per calorimeter detector. The timing of the upstream and downstream PMTs separately can be determined using the difference and additional assumptions about the walk corrections and the distribution of particles in the BGV.

A.3 Note on Walk-Corrections

In the previous sections we have assumed that the time slewing of pulses due to walk in the leading-edge discriminators are given by a function f_w which is commonly taken to be given by the formula in Eq. 15:

$$f_w(a; T, C_{walk}) = C_{walk}\left(\sqrt{\frac{T}{a}} - \sqrt{\frac{T}{a_0}}\right) \qquad (15)$$

The pedestal-subtracted ADC is given by a, the discriminator threshold is represented by T (fixed for the experiment), and the correction is adjusted to be zero at a nominal pulse height a_0. We note that a more accurate parameterization can be used if there is a method of determining its form.